Nuclear Inst, and Methods in Physics Research B 416 (2018) 110–118

Contents lists available at ScienceDirect

Nuclear Inst. and Methods in Physics Research B

journal homepage: www.elsevier.com/locate/nimb

L x-ray production cross sections in high-Z atoms by 3–5 MeV/u silicon ions

M. Oswal[a,b], Sunil Kumar[c], Udai Singh[c,d], G. Singh[e], K.P. Singh[b], D. Mehta[b], D. Mitnik[f], C.C. Montanari[f], T. Nandi[g,*]

[a] Department of Physics, Dev Samaj College, Sec 45-B, Chandigarh 160047, India
[b] Department of Physics, Panjab University, Chandigarh 160014, India
[c] Department of Applied Sciences, Chitkara University, Himachal Pradesh 174103, India
[d] The Marian Smoluchowski Institute of Physics, Jagiellonian University, Lojasiewicza 11, 30-348 Krakow, Poland
[e] Department of Physics, Punjabi University, Patiala, Punjab 147002, India
[f] Instituto de Astronomía y Física del Espacio, CONICET and Universidad de Buenos Aires, Buenos Aires, Argentina
[g] Inter-University Accelerator Centre, JNU New Campus, New Delhi 110067, India

ARTICLE INFO

Keywords:
L-shell x-rays
Heavy ions
Ionization
Multiple-ionization

ABSTRACT

Total L x-ray production cross sections have been measured in $_{74}$W, $_{79}$Au, $_{82}$Pb, and $_{83}$Bi by impact of 3–5 MeV/u ^{28}Si ions, with different charge states q = 8$^+$ up to 12$^+$. We find that the measured cross sections do not differ with the charge state of the projectile ions, but they vary with the beam energies. The experimental data has been compared with three theoretical results, ECUSAR, ECPSSR and SLPA by using the multiple-hole fluorescence and Coster-Kronig yields. The comparison has showed the best agreement with the ECUSAR. The SLPA results also describe the experiments quite well for $_{74}$W, $_{79}$Au and $_{83}$Bi, but certain differences are observed for $_{82}$Pb, while the ECPSSR values underestimate by up to a factor two. Surprisingly, the theoretical-experimental agreement is better at low beam energies than in the high beam energy side.

1. Introduction

The measurement of inner-shell ionization of heavy targets by ion impact has led to advances in radiation [1], plasma [2], atomic and nuclear physics [3], and in particle induced x-ray emission (PIXE) technique [4,5]. Since the inception, PIXE mostly has made use of the light ions such as protons and alphas [6–16], nevertheless the use of heavy ions for the PIXE analysis is increasing due to advantage of higher cross sections and hence the scope of achieving the better sensitivity [17]. Discrepancies observed between the theories and experiments have often been ascribed to the multiple ionization even experiments done with the protons [18]. Though the multiple-ionization effect has been known for a long while in L-shell ionization by the heavy ion impacts [19–35], however, this effect is still rarely used in the analysis for the x-ray emission in view of the elemental analysis.

The inner shell ionization of a target (atomic number Z_T) by a projectile (atomic number Z_P) is the effect of two contributions: the direct ionization (DI) (a target bound electron ends in the continuum) and the electron capture (EC) (electron transfer from the target to a bound state of the projectile). In asymmetric collisions, $Z_P/Z_T \ll 1$, the DI is the main contribution, while for symmetric collisions, $Z_P/Z_T \sim 1$, the EC is also important. In this contribution we have the double aim of contributing to the experimental knowledge of the L-shell ionization of very heavy targets (W, Au, Pb and Bi) by a heavy ion (^{28}Si); and for a meaningful comparison with existing ionization theories. We selected two completely different formalisms for the theoretical comparison, the well-known ECPSSR [36] and ECUSAR [37] theories, within the binary collisional formalism, and the shellwise local plasma approximation (SLPA) [38,39], which is a many electron model within the dielectric formalism. The collisional systems measured here correspond to asymmetric collisions, i.e. $0.15 \leq Z_P/Z_T \leq 0.18$, but less asymmetric than that used for a previous work [35].

In Section 2, we present the experimental description for the L x-ray production cross-sections in thin solid targets ionized by the swift ^{28}Si ions. The impact velocities are much lower than the orbital velocity of the L-shell electrons in the target atom, $v_T = (Z_T–4.15)/2$ and the velocity ratio v_P/v_T remains in the bound $0.026 \leq v_P/v_T \leq 0.043$. In Section 3, we briefly describe and comment on the theoretical models considered in the present work. Section 4 gives the effects of the single- and multiple-hole atomic parameters required for conversion of the ionization cross sections to the x-ray production cross sections, and Section 5 summarizes the results.

* Corresponding author.
E-mail address: nanditapan@gmail.com (T. Nandi).

https://doi.org/10.1016/j.nimb.2017.11.025
Received 27 September 2017; Received in revised form 10 November 2017; Accepted 27 November 2017
Available online 04 January 2018
0168-583X/

2. Experimental details and data analysis

The L x-ray production cross sections were measured in the $_{74}$W, $_{79}$Au, $_{82}$Pb, and $_{83}$Bi elements by the ^{28}Si ions (charge states = 8+ and 12+) in the energy range 84–140 MeV. The measurements were performed using the 15 UD Pelletron accelerator at Inter-University Accelerator Centre (IUAC), New Delhi. Pure (99.99%) targets of $_{79}$Au, $_{82}$Pb, and $_{83}$Bi (thickness 120 μg/cm^2) were prepared on the 20 μg/cm^2 carbon backing using the vacuum deposition technique [40]. Thin and spectroscopically pure (99.999%) targets of $_{74}$W with 193 μg/cm^2 on Mylar backing (3 μm), procured from Micromatter, Deer Harbor, Washington, USA was also used in the present work. The energy loss for the incident beam within the target was negligibly small for the target thickness and beam energies used in the present work. Estimated the energy loss by projectile ion in the target material was < 0.5% in most cases except ~1% for $_{74}$W at 84 MeV only. A Si(Li) solid state detector (thickness = 5 mm, diameter = 10 mm, 25 μm Be window from ORTEC, Oak Ridge, Tennessee, USA) was placed in the horizontal ion beam plane configuration outside the vacuum chamber at an angle of 125° to the beam direction and a distance of 170 mm from the target. In the energy range of the measured L x-ray spectra, the energy resolution of the detector was ~200 eV for the Mn Kα x rays. The energy calibration of the detector was performed before and after the measurements using the radioactive ^{55}Fe, ^{57}Co and ^{241}Am sources. The chamber was maintained with a pressure about 10^{-6} Torr. Details of the experimental setup are given in Kumar et al. [35].

A typical L x-ray spectrum from the elemental target of $_{82}$Pb ionized by the 140 MeV ^{28}Si ions is shown in Fig. 1. The spectrum exhibits peaks corresponding to the ionized Li (i = 1–3) subshells. The intense components of the x rays for the elements, viz., Lℓ, Lα1,2, and Lβ2,15 from the L3 subshell, the Lη, Lβ1 and Lγ1,5 from the L2 subshell, and the Lβ3,4 and Lγ2,3 from the L1 subshell, are labeled in the spectrum. The spectrum in semi-log plot shows the weak appearance of Lη and Lγ5. The ratios of net counts for all the lines to the background counts as subtracted by the exponential background (dashed curve) from the spectrum are 0.443, 0.038, 0.096, and 0.215 for Lℓ, Lα, Lβ, and Lγ, respectively. Fig. 2 shows L x-ray spectra of $_{74}$W, $_{79}$Au, $_{82}$Pb, and $_{83}$Bi target excited by the ^{28}Si ion beam at 107 MeV energies. The fluorescence transitions from the Li subshells along with the x-ray energies for various elements are given in Table 1.

The L x-ray production cross section is calculated using the

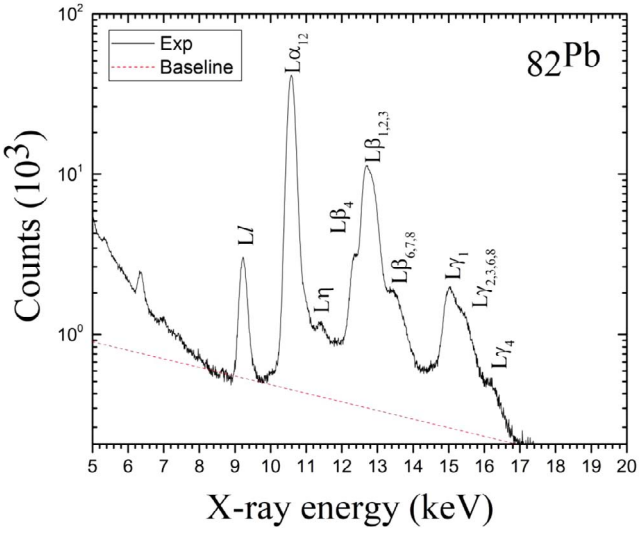

Fig. 1. L x-ray spectra of $_{82}$Pb bombarded with the 140 MeV ^{28}Si ions. The dashed curve exhibits the background due to Compton scattering in the relatively thick (5 mm) detector. As discussed in Section 2, the background amount to < 9% of extracted net x-ray counts except the Lℓ and Lγ line.

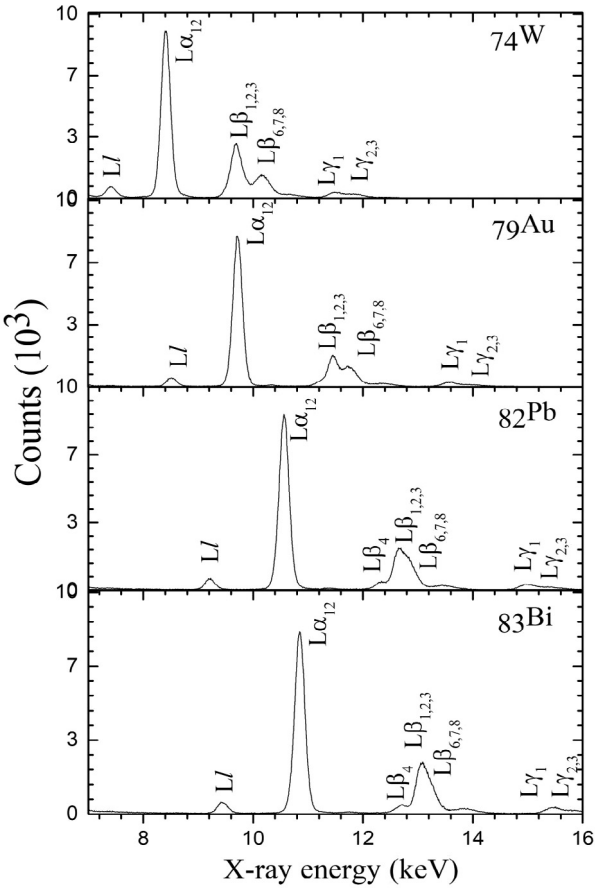

Fig. 2. L x-ray spectra from $_{74}$W, $_{79}$Au, $_{82}$Pb, and $_{83}$Bi bombarded with 107 MeV ^{28}Si ions.

Table 1
L x-ray fluorescence transition along with the energies for various elements used in the present work.

Fluorescence transition (subshell)	x-ray Energy (keV)			
	$_{74}$W	$_{79}$Au	$_{82}$Pb	$_{83}$Bi
Lℓ (L_3)	7.387	8.494	9.184	9.420
Lα$_{1,2}$ (L_3)	8.367	9.671	10.501	10.786
Lη (L_2)	8.724	10.309	11.349	11.712
Lβ$_1$ (L_2)				
Lβ$_3$ (L_1)	9.674	11.431	12.593	12.999
Lβ$_4$ (L_1)	9.524	11.024	12.306	12.69
Lβ$_{2,15}$ (L_3)	9.956	11.576	12.612	12.968
Lγ$_{1,5}$ (L_2)	11.286	13.382	14.765	15.248
Lγ$_{2,3,4}$ (L_1)	11.784	13.939	15.365	15.863

following relation:

$$\sigma_i^x = \frac{Y_i^x A \mathrm{Sin}\theta}{N_A \varepsilon_p n_p t \beta} \quad (1)$$

where Y_i^x is the intensity of the ith x-ray peak, A is the atomic weight of the target, θ is the angle between the ion beam and the target, N_A is the Avogadro's number, $\sigma_i^x(E)$ (in cm^2) is the x-ray production cross section of ith x-ray line at the incident projectile energy (E), ε_p is the absolute detector efficiency, including the absorbing component of Mylar foil used at the window as shown in Fig. 3, and n_p is the number of incident projectiles. Since the inner-shell ionization also depends on the charge state (q) of the projectile ion because for the bare projectiles with no K shell electron or projectile ions with one K shell vacancy, the electron capture contributes considerably to the ionization, whereas, capture is not much while low positive charge states are used for the incident ions;

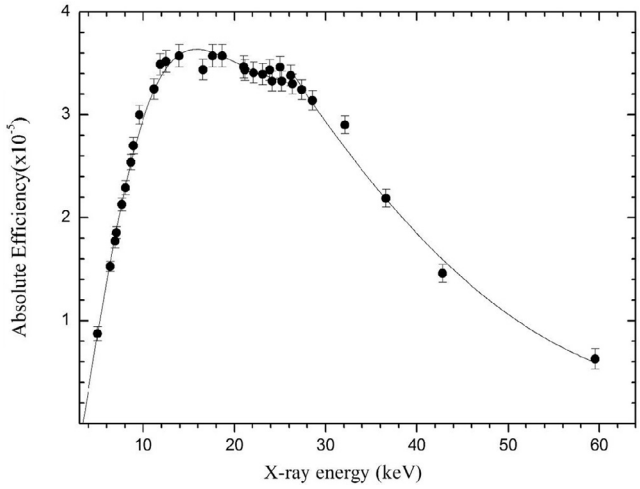

Fig. 3. Efficiency curve obtained by measuring the K x-ray fluorescence yields from targets excited by the 59.54 keV γ-ray photons. Measured values were normalized to absolute efficiency obtained using the calibrated ^{137}Cs and ^{155}Eu radioactive sources.

at this juncture direct ionization is the dominating process. The ion beam changes its charge state during its passage through the target. The mean charge state of the ion beam during the passage through the target and its backing is calculated using the computer code ETACHA [41] and has been used in the analysis.

In the present measurements the peak areas, Y_i^x, are evaluated using the computer program **CANDLE** [42]. In this program, a non-linear least squares fitting routine involving fitting of multiple-Gaussian functions plus a polynomial background is used. This program has the option of fixing the peak centroid and FWHM, and background parameters. This software uses an enhanced version of Levenburg-Marquardt [43] non-linear minimization algorithms for peak fitting. The FWHM for the intrinsic Lorentzian broadening associated with the *L* x-ray lines is < 12 eV [44] compared with ~200 eV for the Gaussian response function of the Si(Li) detector in the energy region of interest.

The percentage error in the measured x-ray production cross sections is about 10–15%. This error is attributed to the uncertainties in different parameters used in the analysis, namely, the photopeak area evaluation (~5% for the Lℓ x-ray peak and 3% for the other peaks), ion beam current (~7%), target thickness (~3%). The error in the absolute efficiency values, ε, is 5–8% in the energy region of interest.

3. Ionization theories

The ECPSSR [36] model by Brandt and Lapicki [36] and its evolution into the ECUSAR model [37] are the most employed theories to describe inner-shell ionization cross sections. They cover an extended energy range, and are the usual input in PIXE codes (see [45]). The ECPSSR theory goes beyond the plane-wave Born approximation (PWBA) by accounting for the energy loss (E), the Coulomb deflection from a straight-line trajectory and retardation of the projectile (C) and its influence on the unperturbed and nonrelativistic atomic orbitals in a perturbed stationary state (PSS) treatment that also accounts for the relativistic (R) nature of the inner shells of heavy target atom. In the ECUSAR theory [37], Lapicki replaces the PSS treatment of ECPSSR with united (U) and separated (S) atom (A) formula (see Eqs. (2), (3) in [37]).

Similar to the PWBA, the ECPSSR and ECUSAR theories describe the binary collision between the projectile and an electron of the target in an hydrogen-like potential. To have a different and independent theoretical comparison with our present measurements, we resorted to the shellwise local plasma approximation (SLPA) [38,39]. The SLPA is an *ab initio* many-electron model within the frame of the dielectric formalism, especially suitable for multi-electronic targets and intermediate to high energy collisions. The SLPA describes the collective response of each subshell of target electrons as a whole, including screening and correlation among electrons. The ionization probabilities are calculated through a dielectric function for each subshell of target electrons, characterized by their electronic density and binding energy (an electron gas with an energy threshold). For W, Au, Pb and Bi we employed the relativistic wave functions and binding energies of the ground state of these atoms as in [39]. This allowed us to account for the spin-orbit split in energy for the different Li (i = 1–3) ionization cross sections. The SLPA ionization cross-section of the Li subshell due to the interaction with an ion of impact velocity *v*, nuclear charge Z_P, *N* bound electrons and charge state $q = Z_P - N$ is given by

$$P_{Li}^{SLPA} = \frac{2}{\pi v^2}\int_0^\infty Z_q^2(k)\frac{dk}{k}\int_0^{kv} d\omega \int d\vec{r}\,\mathrm{Im}\left[\frac{-1}{\varepsilon_{Li}(k,\omega,\delta_{Li}(r),E_{Li})}\right] \quad (2)$$

where δ_{Li} and E_{Li} are the electronic density and binding energy, and ε_{Li} is Levine-Louie dielectric function [38]. We calculated the $Z_q(k)$ for the different charge states of the Si ions as in the appendix of [39], using the Hartree Fock wave functions of the Si bound electrons for the different positive ions by Clementi-Roetti [46]. The ion bound electrons screen the Coulomb potential of the projectile. The Fourier transform of this screened potential is $V(k) = -4\pi Z_q(k)/k^2$, with $Z_q(k)\xrightarrow[k\to\infty]{} Z_P$ for close collisions (large *k*), and $Z_q(k)\xrightarrow[k\to 0]{} q = Z_P - N$ for long distance collisions ($k \to 0$). This is very important for the results obtained here, as we will note later in this work. Although we performed the detailed calculation for each charge state of the Si ions, as we deal with very deep subshells, the theoretical values obtained are quite similar to just considering the interaction with $Z_P = +14$.

The theoretical *L* x-ray production cross sections for the most commonly resolved *Lℓ*, *Lα*, *Lβ*, *Lη*, and *L*γ x rays are related to the L_i subshell ionization cross sections, σ_{Li}, as given below

$$\sigma_{Ll} = [\sigma_{L1}(f_{12}f_{23} + f_{13}) + \sigma_{L2}f_{23} + \sigma_{L3}]\omega_3 F_{3l} \quad (3a)$$

$$\sigma_{L\alpha}^x = [\sigma_{L1}(f_{12}f_{23} + f_{13}) + \sigma_{L2}f_{23} + \sigma_{L3}]\omega_3 F_{3\alpha} \quad (3b)$$

$$\sigma_{L\eta}^x = [\sigma_{L1}f_{12} + \sigma_{L2}]\omega_2 F_{2\eta} \quad (3c)$$

$$\sigma_{L\beta}^x = \sigma_{L1}[\omega_1 F_{1\beta} + f_{12}\omega_2 F_{2\beta} + (f_{12}f_{23} + f_{13})\omega_3 F_{3\beta}] + \sigma_{L2}(\omega_2 F_{2\beta} + f_{23}\omega_3 F_{3\beta}) + \sigma_{L3}\omega_3 F_{3\beta} \quad (3d)$$

$$\sigma_{L\gamma}^x = \sigma_{L1}(\omega_1 F_{1\gamma} + f_{12}\omega_2 F_{2\gamma}) + \sigma_{L2}\omega_2 F_{2\gamma} \quad (3e)$$

where $\sigma_{Lp}^x (p = l, \alpha, \beta, \gamma, \eta)$ are the x-ray production cross sections of the different *L* x-ray components,σ_{Li} (i = 1–3) the ionization cross sections for the L_1, L_2, and L_3 subshells, ω_i (i = 1–3) are the fluorescence yields of the L_i subshells, f_{ij} ($i < j$) the CK yields for the CK transition between the L_i and L_j subshells, and F_{ip} (i = 1–3, $p = l, \alpha, \beta, \gamma, \eta$) are the fractional radiative emission rates.

The theoretical L x-ray production cross sections were calculated by combining the Li (i = 1–3) ionization cross sections obtained by the ECPSSR [36], the ECUSAR [37], and SLPA [38,39] approximations in Eqs. (3a)–(3e). The measured L x-ray production cross-sections and the calculated ones from the different theories including the correction for the multiple ionization (MI) effects, viz., ECPSSR-MI, and ECUSAR-MI, and SLPA-MI are given in Table 2. The L x-ray emission rates based on DHS calculation [47] and the interpolated values by Campbell and Wang [48] have been used in the present measurements. For the two datasets of $F_{3\beta}$, $F_{1\gamma}$, and $F_{2\gamma}$ values, the difference is 5–8% over the atomic range Z_T = 50–92, whereas, other values of the emission rates differ from each other by < 4%. The single-hole fluorescence ω_i^0 and CK yields f_{ij}^0 can be obtained from Krause [49] and Chen et al. [50]. The datasets of ω_i^0 and fij^0 differ from each other significantly and are given in Table 3. For the present elements under consideration, the recommended values [48] f_{13}^0(Rec.) are on the average about 15% lower than the f_{13}^0(DHS) ones [47] and ~9% higher than the f_{13}^0(Krause) values [49]. The f_{12}^0 (Rec.) values differ ~15% in average

Table 2
The $L\ell$, $L\alpha$, $L\beta$, $L\gamma$, and total L x-ray production cross section (barn) in elements with $74 \le Z_T \le 83$ bombarded with ^{28}Si ions as measured and calculated with ionization cross sections according to the ECPSSR-MI [36], ECUSAR-MI [37] and SLPA-MI [38,39] theories converted to x-ray production cross sections with atomic parameters modified for multiply-ionized (MI) elements [53]. The ratios of the measured to calculated cross sections are listed in the parenthesis. In bold prints are the best agreements between experiment and theory. The ECUSAR theory shows the best representation of the experiments and second best is the SLPA. ECPSSR predictions are within a factor of two. Experimental uncertainty varies within 10–15%.

Element	^{28}Si ion beam		x-ray production cross sections (barns/atom)			
	Energy (MeV)	Charge state	Experiment	ECUSAR-MI [37]	ECPSSR-MI [36]	SLPA-MI [38,39]
$_{74}W$						
$L\ell$ x-ray	84	8^+	295	**273(0.93)**	138(0.47)	316(1.07)
	90	8^+	333	**323(0.97)**	158(0.47)	360(1.08)
	98	8^+	427	395(0.93)	186(0.44)	**421.74(0.99)**
	107	8^+	509	483(0.95)	219(0.43)	**494.8(0.97)**
	118	12^+	982	**772(0.79)**	585(0.60)	733.84(0.75)
	128	12^+	1106	**889(0.80)**	668(0.60)	821.93(0.74)
	140	12^+	1268	**1033(0.81)**	769(0.61)	932.39(0.74)
$L\alpha$ x-ray	84	8^+	6390	5827(0.91)	2942(0.46)	**6753(1.06)**
	90	8^+	7115	**6897(0.97)**	3369(0.47)	7698(1.08)
	98	8^+	9134	8441(0.92)	3967(0.43)	**9010(0.99)**
	107	8^+	10,819	10,320(0.95)	4670(0.43)	**10,571(0.98)**
	118	12^+	20,964	**16,489(0.79)**	12,504(0.60)	15,677(0.75)
	128	12^+	23,658	**18,996(0.80)**	14,271(0.60)	17,559(0.74)
	140	12^+	26,688	**22,070(0.83)**	16,438(0.62)	19,919(0.75)
$L\beta$ x-ray	84	8^+	3478	3173(0.91)	1734(0.50)	3673(1.06)
	90	8^+	3899	**3813(0.98)**	2022(0.52)	4345(1.11)
	98	8^+	5124	4764(0.93)	2436(0.48)	**5304(1.04)**
	107	8^+	6189	**5956(0.96)**	2934(0.47)	6477(1.05)
	118	12^+	12,367	9808(0.79)	7753(0.63)	**10,170(0.82)**
	128	12^+	14,217	11,553(0.81)	9042(0.64)	**11,750(0.83)**
	140	12^+	16,303	**13,747(0.84)**	10,652(0.65)	13,743(0.84)
$L\gamma$ x-ray	84	8^+	435	**427(0.98)**	248(0.57)	510(0.96)
	90	8^+	534	**520(0.97)**	294(0.55)	619(0.86)
	98	8^+	720	**661(0.92)**	360(0.50)	778(0.89)
	107	8^+	871	**842(0.97)**	441(0.51)	973(0.56)
	118	12^+	1732	1424(0.82)	1159(0.67)	**1589(0.92)**
	128	12^+	2026	1705(0.84)	1372(0.68)	**1865(0.92)**
	140	12^+	2412	2062(0.85)	1641(0.68)	**2214(0.92)**
L x-ray	84	8^+	10,598	9700(0.92)	5062(0.48)	**11,252(1.06)**
	90	8^+	11,881	**11,553(0.97)**	5843(0.49)	13,023(1.10)
	98	8^+	15,405	14,261(0.93)	6949(0.45)	**15,513(1.01)**
	107	8^+	18,388	17,601(0.96)	8264(0.45)	**18,516(1.01)**
	118	12^+	36,045	**28,493(0.79)**	22,001(0.61)	28,170(0.78)
	128	12^+	41,007	**33,143(0.81)**	25,353(0.62)	31,995(0.78)
	140	12^+	46,671	**38,912(0.83)**	29,500(0.63)	36,808(0.79)
$_{79}Au$						
$L\ell$ x-ray	84	8^+	180	**177(0.98)**	94(0.52)	185(1.03)
	90	8^+	220	211(0.96)	109(0.50)	**215(0.98)**
	98	8^+	265	**261(0.98)**	130(0.49)	257(0.97)
	107	8^+	327	**324(0.99)**	155(0.47)	308(0.94)
	118	12^+	567	**508(0.90)**	397(0.70)	452(0.80)
	128	12^+	699	**596(0.85)**	461(0.66)	516(0.74)
	140	12^+	842	**707(0.84)**	542(0.64)	597(0.71)
$L\alpha$ x-ray	84	8^+	3578	**3515(0.98)**	1870(0.52)	3682(1.03)
	90	8^+	4365	4195(0.96)	2163(0.50)	**4275(0.98)**
	98	8^+	5260	**5194(0.99)**	2579(0.49)	5107(0.97)
	107	8^+	6543	**6435(0.98)**	3080(0.47)	6126(0.94)
	118	12^+	11,311	**10,102(0.89)**	7896(0.70)	8981(0.79)
	128	12^+	13,822	**11,848(0.86)**	9163(0.66)	10,258(0.74)
	140	12^+	16,678	**14,053(0.84)**	10,767(0.65)	11,877(0.71)
$L\beta$ x-ray	84	8^+	1858	**1834(0.99)**	1027(0.55)	1754(0.94)
	90	8^+	2290	**2210(0.97)**	1202(0.52)	2103(0.92)
	98	8^+	2804	**2770(0.99)**	1455(0.52)	2621(0.93)
	107	8^+	3522	**3481(0.99)**	1764(0.50)	3262(0.93)
	118	12^+	6277	**5601(0.89)**	4513(0.72)	5076(0.81)
	128	12^+	7826	**6676(0.85)**	5322(0.68)	5975(0.76)
	140	12^+	9604	**8060(0.84)**	6361(0.66)	7117(0.74)
$L\gamma$ x-ray	84	8^+	249	**246(0.99)**	144(0.58)	222(0.89)
	90	8^+	307	**299(0.97)**	170(0.55)	275(0.90)
	98	8^+	384	**379(0.99)**	209(0.54)	356(0.93)
	107	8^+	489	**482(0.99)**	257(0.53)	457(0.93)
	118	12^+	888	**796(0.90)**	657(0.74)	749(0.84)
	128	12^+	1122	**962(0.86)**	786(0.70)	900(0.80)
	140	12^+	1403	**1179(0.84)**	952(0.68)	1093(0.78)
L x-ray	84	8^+	5865	5772(0.98)	3135(0.53)	**5844(1.00)**
	90	8^+	7182	**6915(0.96)**	3644(0.51)	**6867(0.96)**
	98	8^+	8713	**8604(0.99)**	4373(0.50)	8341(0.96)
	107	8^+	10,881	**10,722(0.99)**	5256(0.48)	10,154(0.93)

(*continued on next page*)

Table 2 (*continued*)

Element	^{28}Si ion beam		x-ray production cross sections (barns/atom)			
	Energy (MeV)	Charge state	Experiment	ECUSAR-MI [37]	ECPSSR-MI [36]	SLPA-MI [38,39]
	118	12^+	19,043	**17,007(0.89)**	13,463(0.71)	15,258(0.80)
	128	12^+	23,469	**20,082(0.86)**	15,732(0.67)	17,650(0.75)
	140	12^+	28,527	**23,999(0.84)**	18,622(0.65)	20,685(0.73)
$_{82}$Pb						
Lℓ x-ray	84	8^+	177	**136(0.77)**	74(0.42)	58(0.33)
	90	8^+	190	**162(0.85)**	86(0.45)	78(0.41)
	98	8^+	214	**202(0.94)**	103(0.48)	109(0.51)
	107	8^+	331	**251(0.76)**	123(0.37)	153(0.46)
	118	12^+	501	**392(0.78)**	311(0.62)	189(0.38)
	128	12^+	614	**463(0.75)**	364(0.59)	251(0.41)
	140	12^+	686	**554(0.81)**	430(0.63)	332(0.48)
Lα x-ray	84	8^+	3404	**2573(0.76)**	1402(0.41)	1097(0.32)
	90	8^+	3555	**3081(0.87)**	1627(0.46)	1471(0.41)
	98	8^+	3964	**3830(0.97)**	1949(0.49)	2076(0.52)
	107	8^+	6341	**4767(0.75)**	2338(0.37)	2896(0.46)
	118	12^+	9974	**7438(0.75)**	5903(0.59)	3584(0.36)
	128	12^+	12,029	**8787(0.73)**	6897(0.57)	4765(0.40)
	140	12^+	13,251	**10,512(0.79)**	8158(0.62)	6292(0.47)
Lβ x-ray	84	8^+	1749	1337(0.76)	760(0.43)	**1908(1.09)**
	90	8^+	1866	**1614(0.86)**	892(0.48)	2291(1.23)
	98	8^+	2098	**2028(0.97)**	1085(0.52)	2861(1.36)
	107	8^+	3391	2558(0.75)	1322(0.39)	**3563(1.05)**
	118	12^+	5361	4074(0.76)	3323(0.62)	**5342(1.00)**
	128	12^+	6577	4889(0.74)	3946(0.60)	**6307(0.96)**
	140	12^+	7529	5952(0.79)	4750(0.63)	**7530(1.00)**
Lγ x-ray	84	8^+	236	**181(0.77)**	107(0.45)	467(1.98)
	90	8^+	259	**220(0.85)**	127(0.49)	549(2.12)
	98	8^+	296	**279(0.94)**	156(0.53)	667(2.25)
	107	8^+	491	**357(0.73)**	193(0.39)	807(1.64)
	118	12^+	789	**581(0.74)**	485(0.61)	1271(1.61)
	128	12^+	971	**708(0.73)**	585(0.60)	1459(1.50)
	140	12^+	1121	**876(0.78)**	715(0.64)	1696(1.51)
L x-ray	84	8^+	5566	**4227(0.76)**	2343(0.42)	3530(0.63)
	90	8^+	5870	**5077(0.86)**	2732(0.47)	4388(0.75)
	98	8^+	6572	**6339(0.96)**	3293(0.50)	5713(0.87)
	107	8^+	10,554	**7933(0.75)**	3976(0.38)	7419(0.70)
	118	12^+	16,625	**12,485(0.75)**	10,022(0.60)	10,386(0.62)
	128	12^+	20,191	**14,847(0.74)**	11,792(0.58)	12,783(0.63)
	140	12^+	22,587	**17,894(0.79)**	14,053(0.62)	15,849(0.70)
$_{83}$Bi						
Lℓ x-ray	84	8^+	144	124(0.86)	68(0.47)	**126(0.88)**
	90	8^+	166	**149(0.90)**	79(0.48)	**149(0.90)**
	98	8^+	204	**186(0.91)**	95(0.47)	181(0.89)
	107	8^+	247	**231(0.94)**	114(0.46)	221(0.89)
	118	12^+	419	**360(0.86)**	287(0.68)	323(0.77)
	128	12^+	479	**426(0.89)**	336(0.70)	375(0.78)
	140	12^+	584	**511(0.88)**	398(0.68)	441(0.76)
Lα x-ray	84	8^+	2823	2325(0.82)	1275(0.45)	**2364(0.84)**
	90	8^+	3182	**2786(0.88)**	1482(0.47)	**2785(0.88)**
	98	8^+	3946	**3468(0.88)**	1777(0.45)	3381(0.86)
	107	8^+	4767	**4322(0.91)**	2135(0.45)	4130(0.87)
	118	12^+	8110	**6728(0.83)**	5365(0.66)	6045(0.75)
	128	12^+	9248	**7966(0.86)**	6280(0.68)	7006(0.76)
	140	12^+	11,314	**9553(0.84)**	7447(0.66)	8249(0.73)
Lβ x-ray	84	8^+	1461	**1207(0.83)**	690(0.47)	1074(0.74)
	90	8^+	1660	**1458(0.88)**	810(0.49)	1318(0.79)
	98	8^+	2084	**1834(0.88)**	986(0.47)	1691(0.81)
	107	8^+	2549	**2315(0.91)**	1203(0.47)	2167(0.85)
	118	12^+	4392	**3673(0.84)**	3007(0.68)	3406(0.78)
	128	12^+	5102	**4417(0.87)**	3578(0.70)	4108(0.81)
	140	12^+	6364	**5390(0.85)**	4318(0.68)	5011(0.79)
Lγ x-ray	84	8^+	197	**163(0.83)**	97(0.49)	130(0.66)
	90	8^+	226	**199(0.88)**	115(0.51)	167(0.74)
	98	8^+	283	**253(0.89)**	142(0.50)	228(0.81)
	107	8^+	355	**323(0.91)**	176(0.50)	308(0.87)
	118	12^+	613	**524(0.85)**	440(0.72)	**519(0.85)**
	128	12^+	735	640(0.87)	531(0.72)	**647(0.88)**
	140	12^+	936	794(0.85)	651(0.70)	**810(0.87)**
L x-ray	84	8^+	4625	**3819(0.83)**	2130(0.46)	3695(0.80)
	90	8^+	5234	**4592(0.88)**	2486(0.47)	4419(0.84)
	98	8^+	6517	**5741(0.88)**	3000(0.46)	5482(0.84)
	107	8^+	7918	**7191(0.91)**	3628(0.46)	6825(0.86)

(*continued on next page*)

Table 2 (*continued*)

Element	^{28}Si ion beam		x-ray production cross sections (barns/atom)			
	Energy (MeV)	Charge state	Experiment	ECUSAR-MI [37]	ECPSSR-MI [36]	SLPA-MI [38,39]
	118	12^+	13,534	**11,285(0.83)**	9099(0.67)	10,293(0.76)
	128	12^+	15,564	**13,449(0.86)**	10,725(0.69)	12,135(0.78)
	140	12^+	19,198	**16,248(0.85)**	12,814(0.67)	14,513(0.76)

higher than the $f_{12}{}^0$(DHS) values [47] and are about half the $f_{12}{}^0$(Krause) values [49]. The $f_{23}{}^0$(Rec.) values [48] from different sets do not differ significantly. The $\omega_2{}^0$(Rec.) and $\omega_3{}^0$(Rec.) values agree with the DHS values and are about 10% higher than the Krause's ones [49] for the present elements. The $\omega_1{}^0$(Rec.) values differ from $\omega_1{}^0$(Krause) values by 0–14% and from $\omega_1{}^0$(DHS) by 13–52%. The use of different sets of atomic parameters can change the x-ray production cross section by ~30%. Recent values of $\omega_i{}^0$ and $f_{ij}{}^0$ compiled by Campbell [51,52] for the elements with $25 \le Z \le 96$ have been used in the present work for singly-ionized atoms.

4. Effect of single and multiple-hole atomic parameters on the conversion of ionization to x-ray production cross sections

Multiple vacancies in the target atom change the atomic parameters by increasing the fluorescence yields and decreasing CK yields which in turn enhances x-ray production cross sections. In the present work, single-hole fluorescence $\omega_i{}^0$ and CK yields $f_{ij}{}^0$ [51], were corrected for multiple ionization using a model prescribed by Lapicki et al. [53] and used in our recent work [35]. Each electron in a manifold of the outer subshells is ionized with a probability P as given below:

$$P = \frac{q^2}{2\beta v_P^2}\left(1-\frac{\beta}{4v_P^2}\right), \quad (4)$$

where $\beta = 0.9$ and we replaced the projectile atomic number Z_P by its charge state q [54]. The $\omega_i{}^0$ values are corrected for simultaneous ionization in outer subshells as

$$\omega_i = \omega_i^o[1-P(1-\omega_i^o)]^{-1}, \quad (5)$$

while the f_{ij} values for the multiple ionization are corrected by

$$f_{ij} = f_{ij}^o(1-P)^2. \quad (6)$$

Note that the fractional rates F_{ip} remain unchanged because both partial and total non-radiative widths are narrowed by identical factors. Following Eqs. (5) and (6), the single-hole fluorescence and CK yields are changed at different ion beam energies and charge states.

Table 4
The fluorescence and CK yields for the singly ionized (SI) and multiply ionized (MI) target elements at the 107 MeV $^{28}Si^{8+}$ ion beam used in the present work.

Atomic number (Z)		Fluorescence yield			CK yield		
		ω_1	ω_2	ω_3	f_{12}	f_{13}	f_{23}
74	SI	0.148	0.291	0.261	0.110	0.333	0.132
	MI	0.184	0.348	0.315	0.065	0.197	0.078
79	SI	0.117	0.358	0.313	0.074	0.615	0.125
	MI	0.147	0.420	0.372	0.044	0.364	0.074
82	SI	0.128	0.397	0.343	0.066	0.620	0.119
	MI	0.160	0.461	0.404	0.039	0.367	0.079
83	SI	0.132	0.411	0.353	0.063	0.620	0.117
	MI	0.165	0.476	0.415	0.037	0.367	0.069

The fluorescence and CK yields for the singly ionized (SI) as well as multiply ionized (MI) target elements by the 107 MeV $^{28}Si^{8+}$ ion beam are displayed in Table 4. It is clear from this table that in the extreme, the L_i subshell fluorescence yields are enhanced by 15%, and the CK yields are reduced by 27% from single-hole to multiple-hole in the $_{82}$Pb atom. We found that these values differ by 2–3% over the range of the ion beam energies and the projectile charge states used in the present experiments. Note that agreement between measured and calculated L_i subshell ionization cross sections depends on how good the theory accounts for intra-shell coupling and inner-shell multiple ionization effects [55,56]. For the ionization data of comparably heavy targets as ours and by significantly ions [57] corroborate our results that the multiple-ionization is more responsible than the intra-shell coupling effects.

5. Results and discussion

In Table 2, we listed the present results for the L-shell line and total x-ray production cross sections for the different impact energies and

Table 3
The fluorescence and CK yields [42] for singly ionized elements used in the present work.

Element	Fluorescence yield								
	ω_1			ω_2			ω_3		
	Rec. [42]	DHS	Krause	Rec. [42]	DHS	Krause	Rec. [42]	DHS	Krause
$_{74}$W	0.148	0.136	0.147	0.291	0.291	0.270	0.261	0.261	0.255
$_{79}$Au	0.117	0.078	0.107	0.358	0.358	0.334	0.313	0.313	0.320
$_{82}$Pb	0.128	0.093	0.112	0.397	0.397	0.373	0.343	0.343	0.360
$_{83}$Bi	0.132	0.098	0.117	0.411	0.411	0.387	0.353	0.353	0.373
Element	CK yield								
	f_{13}			f_{12}			f_{23}		
	Rec. [42]	DHS	Krause	Rec.[42]	DHS	Krause	Rec. [42]	DHS	Krause
$_{74}$W	0.333	0.352	0.280	0.110	0.186	0.170	0.132	0.140	0.133
$_{79}$Au	0.615	0.711	0.530	0.074	0.068	0.140	0.125	0.129	0.122
$_{82}$Pb	0.620	0.708	0.580	0.066	0.054	0.120	0.119	0.123	0.116
$_{83}$Bi	0.620	0.703	0.580	0.063	0.055	0.110	0.117	0.121	0.113

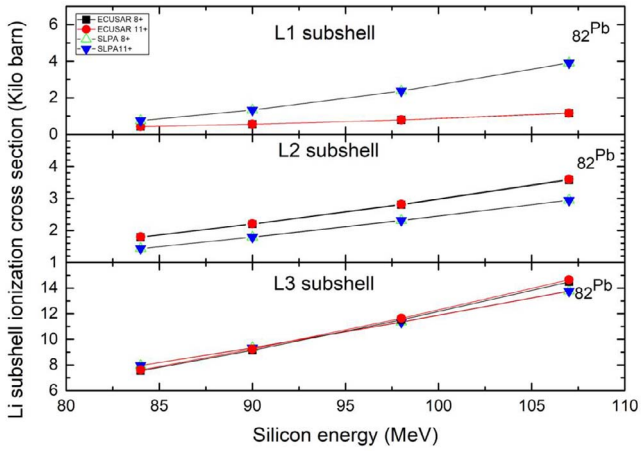

Fig. 4. Li subshell ionization in $_{82}$Pb bombarded by ^{28}Si ions based on the SPLA and ECUSAR theory.

charge states of the silicon ions. We include in this table the experimental L-shell x-ray production cross section measurements and the theoretical predictions by the ECPSSR [36], the ECUSAR [37] and the SLPA [38,39] theories transformed to the x-ray production cross sections using the multiple-hole atomic parameters calculated with the Eqs. (4)–(6), which ignore the effect of the intra-shell coupling. We added –MI to the names in Table 2 to denote that these are not the ionization cross sections of these models, but the combination of them with the multiple ionization parameters. We consider that the intra-shell coupling is negligible in the present conditions and overshadowed by the multiple ionization even in the 3–5 MeV/amu energy range of the present experiments. This is reinforced by the good results displayed in Table 2.

The theoretical ionization cross sections based on the ECUSAR [37], and SLPA [38,39] calculations for the $_{82}$Pb target at different beam energies and charge states of Si ions are shown in Fig. 4. It is clear from the figure that the ionization cross sections over the ion beam energies used in the present work are almost independent of the charge state for the ionization of L_1 subshell and exhibit a slow increasing trend for the L_2 and L_3 subshells with the increasing charge state. Thus, the ionization cross sections mainly depend upon the incident ion energy.

The experimental-theoretical comparison is also shown in Figs. 5–8. The comparisons show best agreement with the ECUSAR and SLPA values, where as the ECPSSR underestimates (in some cases by up to a factor of two. Whereas SLPA-MI represents the experiments quite good for $_{74}$W, $_{79}$Au and $_{83}$Bi, certain differences are observed for $_{82}$Pb. The cross sections are underestimated for the L*l* and Lα and overestimated for Lγ. In contrast, Lβ represent the measurements very well. The SLPA is *ab initio*, it is a completely theoretical description by using the quantum dielectric response theory and the relativistic solutions of the target wave functions and binding energies. This model has already been used to obtain total ionization cross sections of different shells [58–60], even for relativistic targets [39]. But this is the first time the SLPA is employed for the different subshells L_i (2s, $2p_{1/2}$ and $2p_{3/2}$, spin-orbit coupling), so the present agreement is a good test for its ability to deal with these kind of calculations. Based on these considerations, the good description of the experimental values for W, Au and Bi is remarkable, and the strange differences for Pb (Z = 82) will need future research. They are completely unexpected as compared with the good description of Bi (Z = 83), a very similar target.

The experimental total L x-ray cross sections have also been compared with the different theoretical predictions (see Table 2 for each target). We found that the ECUSAR-MI calculation underestimates within 9 to 17%, the SLPA-MI within 14–24% and the ECPSSR-MI by 33–54%. Further, the overall agreement is better at low beam energies than the high beam energy side.

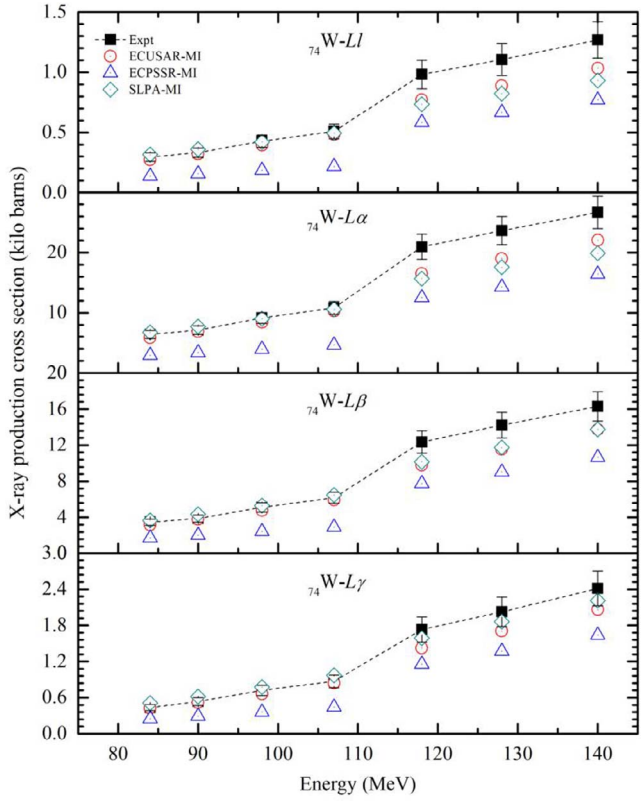

Fig. 5. Ll, Lγ, Lβ and Lα cross sections in $_{74}$W targets bombarded by ^{28}Si ions according to ECUSAR-MI, SLPA-MI and present measurements.

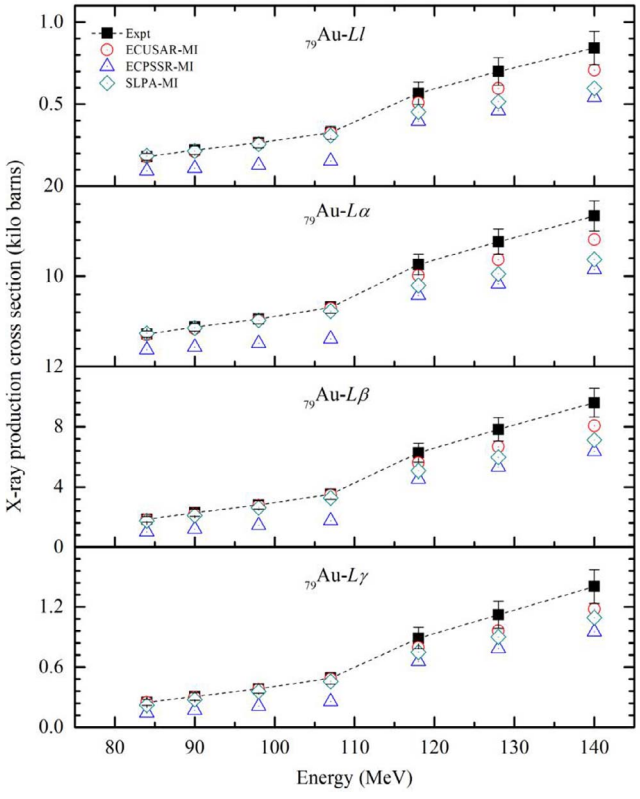

Fig. 6. Ll, Lγ, Lβ and Lα cross sections in $_{79}$Au targets bombarded by ^{28}Si ions according to ECUSAR-MI, SLPA-MI and present measurements.

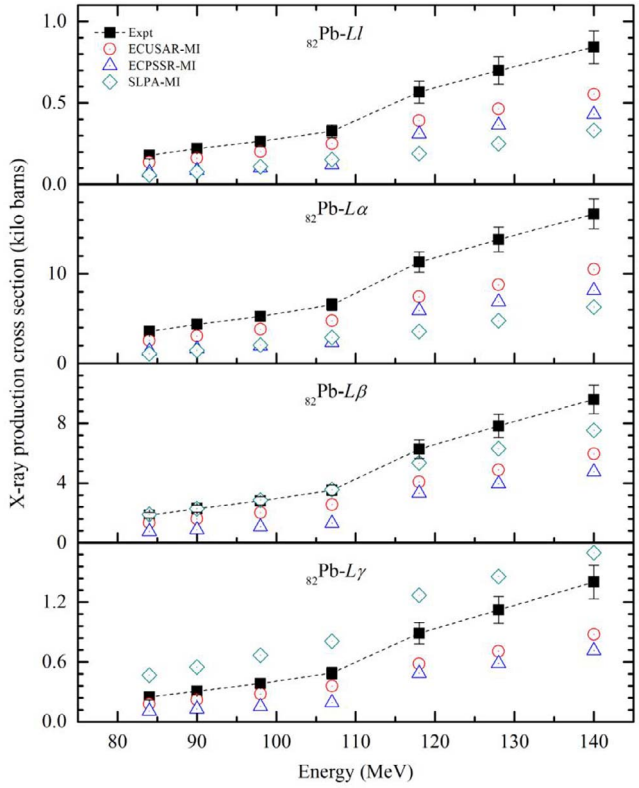

Fig. 7. Ll, Lγ, Lβ and Lα cross sections in $_{82}$Pb targets bombarded by ^{28}Si ions according to ECUSAR-MI, SLPA-MI and present measurements.

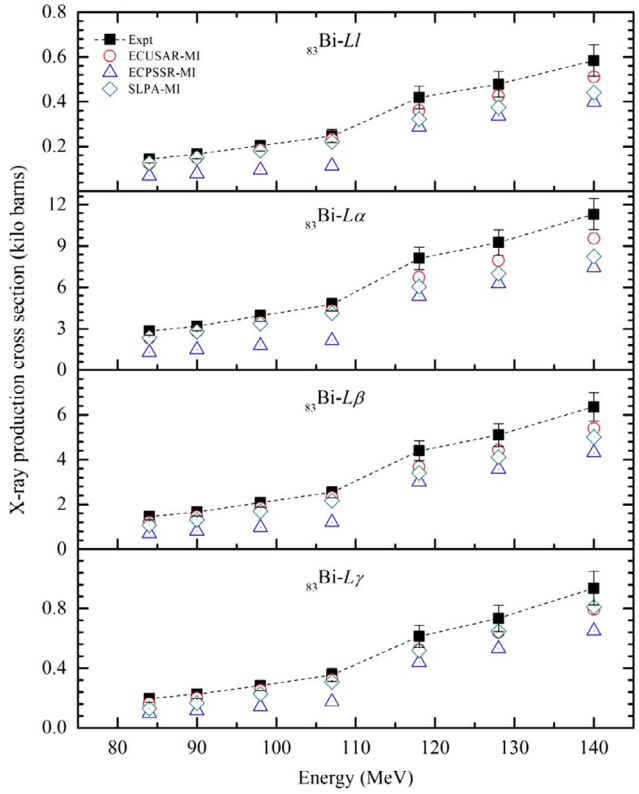

Fig. 8. Ll, Lγ, Lβ and Lα cross sections in $_{83}$Bi targets bombarded by ^{28}Si ions according to ECUSAR-MI, SLPA-MI and present measurements.

6. Conclusions and future prospects

In the present work, the *L* x-ray production cross sections of $_{74}$W, $_{79}$Au, $_{82}$Pb, and $_{83}$Bi target elements by impact of 84–140 MeV ^{28}Si ions (with charge states 8^{+}–12^{+}) have been measured. Theoretical *L* x-ray production cross sections were calculated using the subshell ionization cross sections obtained by using the ECPSSR, ECUSAR and SLPA theories and recently recommended set of the L_i (i = 1–3) subshell fluorescence and CK yields [48] after modification for the multiple vacancies in the outer shells. We found that the measured *L* x-ray production cross sections exhibit best agreement with the ECUSAR-MI and quite good with the SLPA-MI [39] calculations. The measured values are up to two times higher than the ECPSSR-MI. The overall agreement is somewhat better at low beam energies than the high beam energy side. Hence, it appears that the multiple ionization effects have to be tuned further. It is worth mentioning that the ionization cross sections for the ^{28}Si ions with the 8^{+} and 12^{+} charge states over the ion beam energies used in the present work are almost independent of the charge state for the L_1 subshell and exhibit a slow increasing trend for the L_2 and L_3 subshells with the charge states. Thus, the ionization cross sections mainly depend upon the incident ion energy.

The good results obtained with the SLPA considering the different subshells of relativistic targets encourage us to employ this model for targets of even higher atomic numbers in the future. Accurate determination of the *L* x-ray production cross sections of an element with different projectiles is important because of their wide use in the fields of atomic and molecular physics, and non-destructive elemental analysis of materials. Further, better understanding of the basic processes involved in heavy ion induced ionization and fluorescence in presence of the multiple ionization is required and the analytical applications of the heavy ion induced x-ray emission need to be developed for better sensitivity as compared to PIXE technique.

Acknowledgements

Authors acknowledge gratefully G. Lapicki for providing the ECUSAR data. Financial support to Mumtaz Oswal as a research fellow under a research project (KPS) from Department of Science and Technology (DST), New Delhi is highly acknowledged. Another financial support from DST to Sunil Kumar in terms of Young Scientist scheme and a Grant from IUAC, New Delhi in terms of the UF-UP-43302 project are gratefully acknowledged. Authors from Argentina acknowledge the support from CONICET, Agencia Nacional de Promoción Científica y Tecnológica, and Universidad de Buenos Aires. Authors also thank for the service of Pelletron staff for smooth operation of the machine.

References

[1] T. Satoh, Development of particle induced X-ray emission-computed tomography in Takasaki Advanced Radiation Research Institute, Japan Atomic Energy Agency, Int. J. PIXE 25 (2015) 147–152, http://dx.doi.org/10.1142/S0129083515500151.
[2] P. Sharma, T. Nandi, Experimental evidence of beam-foil plasma creation during ion-solid interaction, Phys. Plasmas 23 (2016) 83102, http://dx.doi.org/10.1063/1.4960042.
[3] N.A. Dyson, X-rays in Atomic and Nuclear Physics, 2nd ed., Cambridge University Press, 1990. doi:10.1002/xrs.1300050217.
[4] M. Antoszewska-Moneta, R. Brzozowski, M. Moneta, Modification of thin films induced by slow heavy ions analysed with PIXE and SRIM, Eur. Phys. J. D 69 (2015) 77, http://dx.doi.org/10.1140/epjd/e2015-50629-3.
[5] A.W. Gillespie, C.L. Phillips, J.J. Dynes, D. Chevrier, T.Z. Regier, D. Peak, Advances in using soft X-Ray spectroscopy for measurement of soil biogeochemical processes, Adv. Agron. 133 (2015) 1–32, http://dx.doi.org/10.1016/bs.agron.2015.05.003.
[6] T.B. Johansson, R. Akselsson, S.A.E. Johansson, X-ray analysis: elemental trace analysis at the 10–12 g level, Nucl. Inst. Methods B 84 (1970) 141–143, http://dx.doi.org/10.1016/0029-554X(70)90751-2.
[7] J.D. Garcia, Inner-shell ionizations by proton impact, Phys. Rev. A 1 (1970) 280–285, http://dx.doi.org/10.1103/PhysRevA.1.280.
[8] P. Richard, Ion-atom collisions, Atomic Inner-Shell Processes, Academic Press, New York, 1975, , http://dx.doi.org/10.1007/978-1-4613-2417-1.
[9] D. Joseph, S.V.S. Nageshwara Rao, S. Kailas, Measurement of L X-Ray production cross-sections of Au, Ho, Bi and K-X-Ray cross sections of Nb, Sn, Sb by using

protons of energy 4 MeV, Mapana J. Sci. 12 (2013) 1–8.
[10] X. Zhou, Y. Zhao, R. Cheng, Y. Wang, Y. Lei, X. Wang, Y. Sun, K and L-shell X-ray production cross sections for 50–250 keV proton impact on elements with Z = 26–30, Nucl. Inst. Methods B 299 (2013) 61–67, http://dx.doi.org/10.1016/j.nimb.2013.01.041.
[11] J. Miranda, G. Murillo, B. Méndez, J. López-Monroy, J. Aspiazu, P. Villaseñor, J.C. Pineda, J. Reyes-Herrera, Measurement of L X-ray production cross sections by impact of proton beams on Hf, Ir, and Tl, Nucl. Inst. Methods B 316 (2013) 113–122, http://dx.doi.org/10.1016/j.nimb.2013.08.045.
[12] A.P.L. Bertol, J. Trincavelli, R. Hinrichs, M.A.Z. Vasconcellos, L-shell X-ray production cross sections induced by protons and alpha-particles in the 0.7–2.0 MeV/amu range for Ru and Ag, Nucl. Instr. Methods B 318 (2014) 19–22. doi:10.1016/j.nimb.2013.06.061.
[13] E. Batyrbekov, I. Gorlachev, I. Ivanov, A. Platov, K-, L- and M-shell x-ray production cross sections by 1–1.3 MeV protons, Nucl. Instr. Methods B 325 (2014) 84–88. doi:10.1016/j.nimb.2013.12.025.
[14] J. Miranda G. Lapicki Experimental cross sections for L-shell x-ray production and ionization by protons, At. Data Nucl. Data Tables 100 (2014) 651–780. doi:10.1016/j.adt.2013.07.003.
[15] H. Mohan, A.K. Jain, M. Kaur, P.S. Singh, S. Sharma, Cross section for induced L X-ray emission by protons of energy < 400 keV, Nucl. Instr. Methods B 332 (2014) 103–105, http://dx.doi.org/10.1016/j.nimb.2014.02.039.
[16] A.P.L. Bertol, R. Hinrichs, M.A.Z. Vasconcellos, Proton induced L1, L2, L3-sub-shell X-ray production cross sections of Hf and Au, Nucl. Instr. Methods B 363 (2015) 28–32, http://dx.doi.org/10.1016/j.nimb.2015.08.040.
[17] R. Siegele, D.D. Cohen, N. Dytlewski, The ANSTO high energy heavy ion microprobe, Nucl. Inst. Methods B 158 (1999) 31–38, http://dx.doi.org/10.1016/S0168-583X(99)00393-6.
[18] G.J. Naga, G.A.V. Raju Ramana Murty, B. Seetharami Reddy, T. Seshi Reddy, S. Lakshminarayana, S. Bhuloka Reddy, Multiple ionization effects on L X-ray intensity ratios in Hf, Ta, Re, Ir, Pt, Au and Pb due to proton bombardment at energies 1–5 MeV, Eur. Phys. J. D 30 (2004) 171–179, http://dx.doi.org/10.1140/epjd/e2004-00085-3.
[19] W. Uchai, G. Lapicki, W.T. Milner, S. Raman, P.V. Rao, C.R. Vane, L X-ray emission from high-Z elements after ionisation by 1 MeV u -1 Ag ions, J. Phys. B 18 (1985) L389–L393, http://dx.doi.org/10.1088/0022-3700/18/12/008.
[20] S. Ito, M. Shoji, N. Maeda, R. Katano, T. Mukoyama, R. Ono, Y. Nakayama, L γ X-ray emission in heavy-ion bombardment of Bi, J. Phys. B. 20 (1987) L597–L601, http://dx.doi.org/10.1088/0022-3700/20/18/002.
[21] A. Berinde, C. Ciortea, A. Enulescu, D. Fluerasu, G. Hock, I. Piticu, L. Sarkadi, B. Sulik, V. Zoran, On the L-M-N multiple ionisation in heavy elements, J. Phys. B 20 (1987) L481–L486, http://dx.doi.org/10.1088/0022-3700/20/15/005.
[22] J. Braziewicz, J. Semaniak, T. Czyzewski, L. Glowacka, M. Jaskola, M. Haller, R. Karschnick, W. Kretschmer, D. Trautmann, L-subshell ionization of rare earth elements by carbon ion bombardment, J. Phys. B 27 (1994) 1535–1547, http://dx.doi.org/10.1088/0953-4075/27/8/014.
[23] R. Mehta, H.L. Sun, D.K. Marble, J.L. Duggan, F.D. McDaniel, G. Lapicki, L-shell X-ray production by 2–12 MeV carbon ions in fifteen selected elements from copper to lead, J. Phys. B 28 (1995) 1187–1200, http://dx.doi.org/10.1088/0953-4075/28/7/013.
[24] Y. Yu, C. Wang, E. Lin, T. Liu, L x-ray production in lanthanide elements by 1–5 MeV helium ions, J. Phys. B 30 (1997) 5791–5804, http://dx.doi.org/10.1088/0953-4075/30/24/016.
[25] I. Bogdanović, T. Tadić, M. Jakšić, Z. Halabuka, D. Trautmann, L-shell ionization of Cd, Sb, Te, Ba, La, Eu, Tb and Yb by 16O ions in the energy range from 0.19 to 0.75 MeV u-1, Nucl. Instr. Methods B 150 (1999) 18–26. doi:10.1016/S0168-583X(98)00925-2.
[26] Y.C. Yu, A.R. Azordegan, H.L. Sun, J.L. Duggan, F.D. McDaniel, E.K. Lin, C.W. Wang, G. Lapicki, Charge state dependence of L-shell X-ray production cross sections of 28Ni, 29Cu, 30Zn, 31Ga and 32Ge by 12 MeV 16Oq+ ions, Nucl. Instr. Meth. B. 150 (1999) 27–32. doi:10.1016/S0168-583X(98)01083-0.
[27] D. Mitra, M. Sarkar, D. Bhattacharya, P. Sen, G. Lapicki, L subshell ionisation cross section of gold by 8–15 MeV Si ions, Nucl. Instr. Methods B 152 (1999) 207–211, http://dx.doi.org/10.1016/S0168-583X(99)00016-6.
[28] Y.P. Singh, D. Mitra, L.C. Tribedi, P.N. Tandon, L-subshell ionization of Bi, Au, and Yb induced by F ions at intermediate velocities, Phys. Rev. A 63 (2000) 12713, http://dx.doi.org/10.1103/PhysRevA.63.012713.
[29] D. Banaś, M. Pajek, J. Semaniak, J. Braziewicz, A. Kubala-Kukuś, U. Majewska, T. Czyżewski, M. Jaskóła, W. Kretschmer, T. Mukoyama, D. Trautmann, Multiple ionization effects in low-resolution X-ray spectra induced by energetic heavy ions, Nucl. Instr. Methods B 195 (2002) 233–246, http://dx.doi.org/10.1016/S0168-583X(02)01126-6.
[30] D. Banas, J. Braziewicz, M. Pajek, J. Semaniak, T. Czyżewski, I. Fijal, M. Jaskóla, W. Kretschmer, T. Mukoyama, D. Trautmann, The role of multiple ionization and subshell coupling effects in L-shell ionization of Au by oxygen ions, J. Phys. B 35 (2002) 3421–3433, http://dx.doi.org/10.1088/0953-4075/35/16/305.
[31] M. Pajek, D. Banaś, J. Semaniak, J. Braziewicz, U. Majewska, S. Chojnacki, T. Czyżewski, I. Fijał, M. Jaskóła, A. Glombik, W. Kretschmer, D. Trautmann, G. Lapicki, T. Mukoyama, Multiple ionization and coupling effects in L -subshell ionization of heavy atoms by oxygen ions, Phys. Rev. A 68 (2003) 22705, http://dx.doi.org/10.1103/PhysRevA.68.022705.
[32] M. Czarnota, D. Banaś, M. Berset, D. Chmielewska, J.-C. Dousse, J. Hoszowska, Y.-P. Maillard, O. Mauron, M. Pajek, M. Polasik, P.A. Raboud, J. Rzadkiewicz, K. Słabkowska, Z. Sujkowski, High-resolution X-ray study of the multiple ionization of Pd atoms by fast oxygen ions, Eur. Phys. J. D 57 (2010) 321–324, http://dx.doi.org/10.1140/EPJD/E2010-00039-2.
[33] J. Miranda, G. Murillo, B. Méndez, J. López-Monroy, R.V. Díaz, J. Aspiazu, P. Villaseñor, L-shell X-ray production cross sections of selected lanthanoids by impact of 7Li2+ ions with energies between 3.50MeV and 5.25MeV, Radiat. Phys. Chem. 83 (2013) 48–53, http://dx.doi.org/10.1016/j.radphyschem.2012.09.023.
[34] G. Murillo, B. Méndez, J. López-Monroy, J. Miranda, P. Villaseñor, L-shell X-ray production cross sections of Ce, Nd, Sm, Eu, Gd, and Dy by impact of 14N2+ ions with energies between 7.0 MeV and 10.5 MeV, Nucl. Instr. Methods B 383 (2016) 89–92. doi:10.1016/j.nimb.2016.06.014.
[35] S. Kumar, U. Singh, M. Oswal, G. Singh, N. Singh, D. Mehta, T. Nandi, G. Lapicki, D. M.G. Lapicki, T. Nandi, U. Singh, M. Oswal, G. Singh, N. Singh, D. Mehta, G. Lapicki, T. Nandi, L shell x-ray production in high-Z elements using 4–6 MeV/u fluorine ions, Nucl. Instruments Methods Phys. Res. Sect. B Beam Interact. with Mater. Atoms. 395 (2017) 39–51. doi:10.1016/j.nimb.2017.01.044.
[36] W. Brandt, G. Lapicki, Energy-loss effect in inner-shell Coulomb ionization by heavy charged particles, Phys. Rev. A 23 (1981) 1717–1729, http://dx.doi.org/10.1103/PhysRevA.23.1717.
[37] G. Lapicki, The status of theoretical L-subshell ionization cross sections for protons, Nucl. Instr. Methods B 189 (2002) 8–20, http://dx.doi.org/10.1016/S0168-583X(01)00987-9.
[38] C.C. Montanari, J.E. Miraglia, Theory of heavy ion collision physics in hadron, Therapy (2013), http://dx.doi.org/10.1016/B978-0-12-396455-7.00006-6.
[39] C.C. Montanari, D.M. Mitnik, J.E. Miraglia, A collective model for inner shell ionization of very heavy targets, Radiat. Eff. Defects Solids 166 (2011) 338–345, http://dx.doi.org/10.1080/10420150.2011.572284.
[40] S. Kalkal, S.R. Abhilash, D. Kabiraj, S. Mandal, N. Madhavan, R. Singh, Fabrication of 90,94Zr targets on carbon backing, Nucl. Instr. Methods A 613 (2010) 190–194, http://dx.doi.org/10.1016/j.nima.2009.11.071.
[41] J.P. Rozet, C. Stéphan, D. Vernhet, ETACHA: a program for calculating charge states at GANIL energies, Nucl. Instr. Meths. B. 107 (1996) 67–70, http://dx.doi.org/10.1016/0168-583X(95)00800-4.
[42] E. Subramaniam, B. Kumar, Data acquisition systems-current and future trends, DAE Symp. Nucl. Phys. (2010) 117–120.
[43] D.W. Marquardt, Algorithm for least-squares estimation of nonlinear parameters, J. Soc. Indust. Appl. Math. 11 (1963) 431–441, http://dx.doi.org/10.1017/CBO9781107415324.004.
[44] J.L. Campbell T. Papp, Widths of the atomic K-N7 levels, At. Data Nucl. Data Tables. 77 (2001) 1–56. doi:10.1006/adnd.2000.0848.
[45] G. Lapicki, Werner Brandt legacy to PIXE: past and present perspectives, Nucl. Instr. Methods B 318 (2014) 6–10, http://dx.doi.org/10.1016/j.nimb.2013.05.106.
[46] E. Clementi, C. Roetti, Roothaan-Hartree-Fock atomic wavefunctions. Basis functions and their coefficients for ground and certain excited states of neutral and ionized atoms, Z54 At. Data Nucl. Data Tables 14 (1974) 177–478. doi:10.1016/S0092-640X(74)80016-1.
[47] J.H. Scofield, Relativistic hartree-slater values for K and L X-ray emission rates, At. Data Nucl. Data Tables 14 (1974) 121–137. doi:10.1016/S0092-640X(74)80019-7.
[48] J.L. Campbell, J.X. Wang, Interpolated Dirac-Fock values of L-subshell x-ray emission rates including overlap and exchange effects, At. Data Nucl. Data Tables 43 (1989) 281–291. doi:10.1016/0092-640X(89)90004-1.
[49] M.O. Krause, Atomic radiative and radiationless yields for K and L shells, J. Phys. Chem. Ref. Data 8 (1979) 307–327, http://dx.doi.org/10.1063/1.555594.
[50] M.H. Chen, B. Crasemann, H. Mark, Widths and fluorescence yields of atomic L-shell vacancy states, Phys. Rev. A 24 (1981) 177–182, http://dx.doi.org/10.1103/PhysRevA.24.177.
[51] J.L. Campbell, Fluorescence yields and Coster – Kronig probabilities for the atomic L subshells q, At. Data Nucl. Data Tables. 85 (2003) 291–315. doi:10.1016/S0092-640X(03)00059-7.
[52] J.L. Campbell, Fluorescence yields and Coster-Kronig probabilities for the atomic L subshells. Part II: The L1 subshell revisited, At. Data Nucl. Data Tables 95 (2009) 115–124. doi:10.1016/j.adt.2008.08.002.
[53] G. Lapicki, R. Mehta, J.L. Duggan, P.M. Kocur, J.L. Price, F.D. McDaniel, Multiple outer-shell ionization effect in inner-shell x-ray production by light ions, Phys. Rev. A 34 (1986) 3813–3821, http://dx.doi.org/10.1103/PhysRevA.34.3813.
[54] R. Mehta, J.L. Duggan, F.D. McDaniel, M.R. McNeir, Y. Y.C., D.K. Marble, G. Lapicki, L-shell X-ray production cross sections for 29Cu, 31Ga, 32Ge, 35Br, 39Y, 60Nd, 64Gd, 67Ho, 70Yb, 79Au, and 82Pb for 2–25 MeV carbon ions, Nucl. Inst. Methods B 79 (1993) 175–178. doi:10.1016/0168-583X(93)95318-Y.
[55] L. Sarkadi, L 3 -subshell alignment calculations in the second-order Born approximation for light- and heavy-ion impact on Au, J. Phys. B At. Mol. Phys. 19 (1986) 2519–2530, http://dx.doi.org/10.1088/0022-3700/19/16/011.
[56] M. Sarkar, D. Bhattacharya, M.B. Chatterjee, P. Sen, G. Kuri, D.P. Mahapatra, G. Lapicki, Importance of subshell coupling in L-shell ionization by low-velocity heavy ions, Nucl. Instr. Methods B 103 (1995) 23–27, http://dx.doi.org/10.1016/0168-583X(95)00516-1.
[57] G. Lapicki, G.A.V. Ramana Murty, G.J. Naga Raju, B.S. Reddy, S.B. Reddy, V. Vijayan, Effects of multiple ionization and intrashell coupling in L-subshell ionization by heavy ions, Phys. Rev. A. 70 (2004) 62718, http://dx.doi.org/10.1103/PhysRevA.70.062718.
[58] U. Kadhane, C. Montanari, L. Tribedi, K-shell processes in heavy-ion collisions in solids and the local plasma approximation, Phys. Rev. A. 67 (2003) 1–7, http://dx.doi.org/10.1103/PhysRevA.67.032703.
[59] U. Kadhane, C.C. Montanari, L.C. Tribedi, Experimental study of K-shell ionization of low-Z solids in collisions with intermediate-velocity carbon, J. Phys. B At. Mol. Opt. Phys. 36 (2003) 3043–3054, http://dx.doi.org/10.1088/0953-4075/36/14/307.
[60] U. Kadhane, A. Kumar, C.C. Montanari, L.C. Tribedi, K-shell ionization of low Z elements in ion-solid collisions and applicability of local plasma approximation, Radiat. Phys. Chem. 75 (2006) 1542–1546, http://dx.doi.org/10.1016/j.radphyschem.2005.11.008.